

Spatially separated intrinsic emission components in $\text{In}_x\text{Ga}_{1-x}\text{N}$ ternary alloys

Yoichi Yamada,* Takuya Saito, Nobuo Kato, Eiji Kobayashi, and Tsunemasa Taguchi

Department of Materials Science and Engineering, Yamaguchi University, 2-16-1 Tokiwadai, Ube, Yamaguchi 755-8611, Japan

Hiroimitsu Kudo and Hiroaki Okagawa

Optoelectronics Laboratory, Mitsubishi Chemical Corporation, 1000 Higashimamiana, Ushiku, Ibaraki 300-1295, Japan

(Received 20 March 2009; revised manuscript received 28 July 2009; published 10 November 2009)

The characteristics of band-edge photoluminescence (PL) from Ga-rich $\text{In}_x\text{Ga}_{1-x}\text{N}$ ternary-alloy epitaxial layers with indium compositions of $x=0.02, 0.03, 0.05, 0.06,$ and 0.09 have been comprehensively studied by means of scanning near-field optical microscopy (SNOM) in addition to conventional macroscopic PL spectroscopy. The band-edge PL from the ternary alloys consisted of two intrinsic emission components, a strong higher-energy component and a weak lower-energy component. The radiative recombination channels of the two components were not independent of each other and thermal population of carriers took place between the components. A spatial separation between the two components was clearly indicated by SNOM-PL measurements. The higher-energy component corresponded to islandlike regions with diameters of several hundred nanometers whereas the lower-energy component corresponded to dotlike regions with diameters of 50–80 nm. In addition, the regions corresponding to the lower-energy component were surrounded by a local potential maximum, which acted as a potential barrier for carriers between the higher- and the lower-energy components.

DOI: [10.1103/PhysRevB.80.195202](https://doi.org/10.1103/PhysRevB.80.195202)

PACS number(s): 78.55.Cr, 78.66.Fd, 68.37.Uv

I. INTRODUCTION

Light-emitting devices based on $\text{In}_x\text{Ga}_{1-x}\text{N}$ ternary-alloy semiconductors exhibit high quantum efficiency despite the high density of threading dislocations in the device structures.¹ To date, there has been considerable research carried out on the optical properties of $\text{In}_x\text{Ga}_{1-x}\text{N}$ epitaxial layers and quantum-well (QW) structures using various spectroscopic techniques in order to clarify the radiative recombination mechanism responsible for the high quantum efficiency. Based on experimental observations, the radiative recombination process has been interpreted in terms of carrier or exciton localization at certain potential minima,^{2,3} which results from indium compositional fluctuation.

To investigate the optical inhomogeneity associated with compositional fluctuation and defect distribution in semiconductor alloys and nanostructures, scanning near-field optical microscopy (SNOM) is one of the most powerful tools because it allows subwavelength spatial resolution in photoluminescence (PL) measurements. Several studies on the spatial mapping of the PL from $\text{In}_x\text{Ga}_{1-x}\text{N}$ epitaxial layers and QWs have already been carried out using SNOM.^{4–16} In particular, Hitzel *et al.*¹⁴ reported on a comparison between high- and low-efficiency $\text{In}_x\text{Ga}_{1-x}\text{N}/\text{GaN}$ QWs. They observed regions with larger band gap surrounding defects only in high-efficiency QWs, and these regions were found to act as barriers preventing carriers from recombining nonradiatively at defects. Very recently, Kaneta *et al.*¹⁶ investigated the correlation between the nanoscopic optical and structural properties of $\text{In}_x\text{Ga}_{1-x}\text{N}/\text{GaN}$ QWs by means of SNOM and atomic force microscopy (AFM). They also found that nonradiative recombination centers in blue-emitting QWs were surrounded by energy levels higher than those for radiative recombination centers, and suggested that such potential distributions caused antilocalization of carriers to nonradiative recombination centers, leading to high quantum efficiency in the blue-emitting QWs.

In addition to the studies on real devices based on QW structures, it is also important to study the optical properties of bulk or thick layers of $\text{In}_x\text{Ga}_{1-x}\text{N}$ ternary alloys in order to clarify the intrinsic properties of $\text{In}_x\text{Ga}_{1-x}\text{N}$ itself. We have previously studied the optical characteristics of an $\text{In}_x\text{Ga}_{1-x}\text{N}$ ($x=0.08$) ternary-alloy epitaxial layer.^{17,18} Temperature-dependent and time-resolved PL measurements allowed us to determine that the band-edge PL consisted of two intrinsic emission components.¹⁷ PL excitation (PLE) spectroscopy revealed that the carriers responsible for the two emission components were due to relaxation from the same excited state.¹⁸ We have also studied the optical characteristics of $\text{In}_x\text{Ga}_{1-x}\text{N}$ ternary-alloy epitaxial layers with various indium compositions ($x=0.02, 0.03, 0.05, 0.06,$ and 0.09) by means of optical-absorption (OA) spectroscopy.¹⁹ Temperature-dependent OA measurements allowed us to observe a clear absorption peak up to 300 K, which enabled us to determine the temperature dependence of the Stokes shift. On the basis of our results, it is clear that the radiative recombination process responsible for the band-edge PL of Ga-rich $\text{In}_x\text{Ga}_{1-x}\text{N}$ ternary alloys cannot be explained solely by the simple model of carrier localization due to alloy broadening, which is applicable to most wide-gap II–VI semiconductor ternary-alloy systems. The experimental observations suggest the existence of some other mechanism for carrier localization in $\text{In}_x\text{Ga}_{1-x}\text{N}$ ternary alloys. It is important to identify this mechanism in order to understand the radiative recombination mechanism responsible for high quantum efficiency in $\text{In}_x\text{Ga}_{1-x}\text{N}$ ternary alloys.

In the present work, we first studied the macroscopic optical properties of Ga-rich $\text{In}_x\text{Ga}_{1-x}\text{N}$ ternary-alloy epitaxial layers with indium compositions of $x=0.02, 0.03, 0.05, 0.06,$ and 0.09 by means of excitation-power-density-dependent and temperature-dependent PL spectroscopy. We then investigated the spatial mapping of PL from the ternary alloys by means of SNOM, under the illumination and collection hybrid mode. In particular, we focused on the spatial distribu-

tion of near-field PL for the two intrinsic emission components that dominated the band-edge PL of the ternary alloys.

II. EXPERIMENTAL PROCEDURE

The $\text{In}_x\text{Ga}_{1-x}\text{N}$ epitaxial layers used in the present work were grown by metal-organic vapor phase epitaxy, following the deposition of 5- μm -thick GaN buffer layers on patterned *c*-plane sapphire substrates with parallel grooves along the $\langle 11\text{-}20 \rangle$ direction. The dimensions of the patterned structure were as follows: the width of both ridges and grooves was 3 μm and the depth of grooves was 1.5 μm . The thickness of the $\text{In}_x\text{Ga}_{1-x}\text{N}$ epitaxial layers was 90 nm and the indium composition was varied from $x=0.02$ to 0.09. The indium composition x in $\text{In}_x\text{Ga}_{1-x}\text{N}$ epitaxial layers was estimated by high-resolution x-ray diffraction measurements taking biaxial strain into consideration.²⁰ It was found from plan-view scanning electron microscopy measurements that the distribution of growth pits²¹ was random and was not correlated with the substrate pattern. The density of growth pits in an $\text{In}_{0.05}\text{Ga}_{0.95}\text{N}$ epitaxial layer was estimated to be $1.7 \times 10^8 \text{ cm}^{-2}$. This value agreed with the threading dislocation density of $1.5 \times 10^8 \text{ cm}^{-2}$, which was estimated by plan-view cathodoluminescence (CL) of GaN epitaxial layers on patterned sapphire substrates with the same dimensions mentioned above.²² The surface morphology was also evaluated by means of AFM. The growth pit was also observed in AFM images and the size was about 40–50 nm in diameter. The root-mean-square (rms) roughness of the $\text{In}_{0.05}\text{Ga}_{0.95}\text{N}$ epitaxial layer was 0.388 nm, which was obtained from a $2 \times 2 \mu\text{m}^2$ area including several growth pits. The rms roughness decreased to 0.088 nm when a $500 \times 500 \text{ nm}^2$ area including no growth pits was selected intentionally.

Macroscopic PL was measured using a 325 nm line of a continuous-wave (cw) He-Cd laser as an excitation source. PL spectra were detected by a liquid-nitrogen-cooled charge-coupled-device camera in conjunction with a 50 cm single-grating monochromator with a 2400 grooves/mm grating. The spectral resolution was better than 0.05 nm (i.e., better than 0.4 meV around 3.2000 eV). Near-field PL was measured using a NFS-330 near-field spectrometer (JASCO Co., Ltd.) under the illumination and collection hybrid mode.²³ In this case, both photoexcitation and PL detection were performed through the same optical aperture at the apex of a fiber probe. In this situation, the spatial resolution is limited only by the aperture size. A 325 nm line of a cw He-Cd laser was used as an excitation source. Near-field PL signals collected by an apertured fiber probe were detected by a charge-coupled-device camera in conjunction with a 30 cm single-grating monochromator with a 2400 grooves/mm grating. The spectral resolution was better than 0.23 nm (i.e., better than 1.9 meV around 3.2000 eV).

III. EXPERIMENTAL RESULTS

A. PL spectra at 4 K

Figure 1 shows the PL spectra at 4 K taken from $\text{In}_x\text{Ga}_{1-x}\text{N}$ epitaxial layers with indium compositions of (a) $x=0.02$, (b) $x=0.03$, (c) $x=0.05$, (d) $x=0.06$, and (e) $x=0.09$ under an excitation-power density of 45 W/cm^2 .

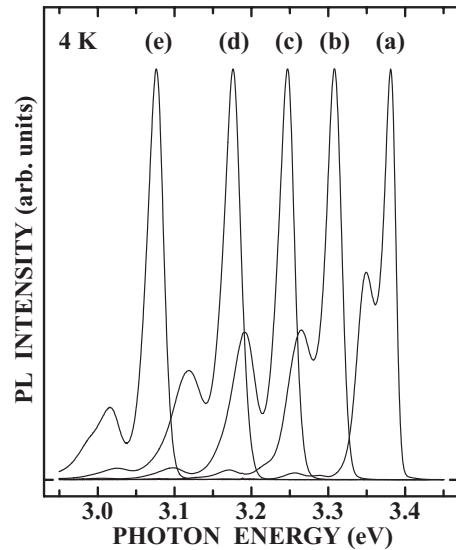


FIG. 1. Photoluminescence spectra at 4 K taken from $\text{In}_x\text{Ga}_{1-x}\text{N}$ epitaxial layers with indium compositions of (a) $x=0.02$, (b) $x=0.03$, (c) $x=0.05$, (d) $x=0.06$, and (e) $x=0.09$ under an excitation-power density of 45 W/cm^2 . Each spectrum is normalized at the peak height of the higher-energy component.

The band-edge PL of each $\text{In}_x\text{Ga}_{1-x}\text{N}$ epitaxial layer is dominated by two emission components: a strong higher-energy component and a weak lower-energy component. Each PL spectrum is normalized at the peak height of the higher-energy component. The ratio of the PL intensity of the lower-energy component to that of the higher-energy component decreases with increasing indium composition. The separation in energy between the higher- and the lower-energy components increases with increasing indium composition from 32 meV for $x=0.02$ to 60 meV for $x=0.09$. In addition, weak PL is observable at the lower-energy side of the two main emission components. The enlarged PL spectrum from the $\text{In}_{0.02}\text{Ga}_{0.98}\text{N}$ epitaxial layer is shown in Fig. 2. The spectrum shown in Fig. 2 is identical to the spectrum shown in Fig. 1(a). At the lower-energy side of the two main emission components, we observed two additional emission components. On the basis of these PL-peak positions, these extra components are attributed to longitudinal optical (LO)-phonon replicas of the main emission components. The energy separation between the main PL component and its LO-phonon replica for both the higher- and the lower-energy components is about 93 meV. It should be noted that the PL intensity of the LO-phonon replica for the lower-energy component is stronger than that for the higher-energy component. We also observed such LO-phonon replicas for the four other samples with higher indium compositions.

B. Excitation-power-density dependence of PL spectra

Figure 3 shows the PL spectra at 4 K taken from the $\text{In}_{0.03}\text{Ga}_{0.97}\text{N}$ epitaxial layer under excitation-power densities of (a) 0.0045, (b) 0.045, (c) 0.23, (d) 0.45, (e) 2.3, (f) 9.0, (g) 23, and (h) 45 W/cm^2 . Each PL spectrum is normalized at the peak height of the higher-energy component. At an excitation-power density of 0.0045 W/cm^2 , the PL spectrum

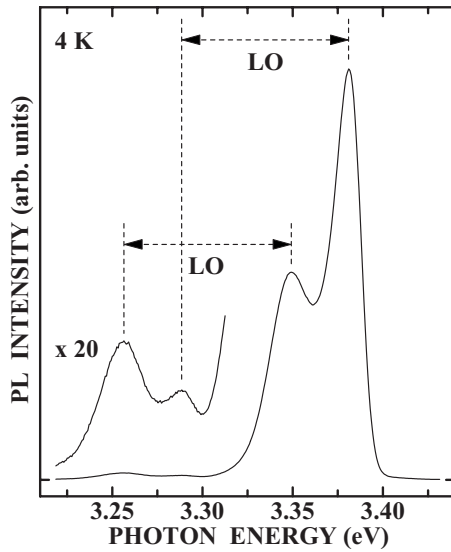


FIG. 2. Enlarged photoluminescence spectrum at 4 K taken from an $\text{In}_{0.02}\text{Ga}_{0.98}\text{N}$ epitaxial layer under an excitation-power density of 45 W/cm^2 .

is dominated by the higher-energy component, and the lower-energy component is negligibly weak. As excitation-power density increases, the PL intensity of the lower-energy component relative to that of the higher-energy component increases rapidly up to 2.3 W/cm^2 . With further increase in excitation-power density, it begins to decrease relative to the higher-energy component. In addition, the lower-energy component, along with its LO-phonon replica, shifts toward higher energy with increasing excitation-power density. In contrast, the position of the higher-energy component remains constant.

Figures 4 and 5 show the excitation-power-density-

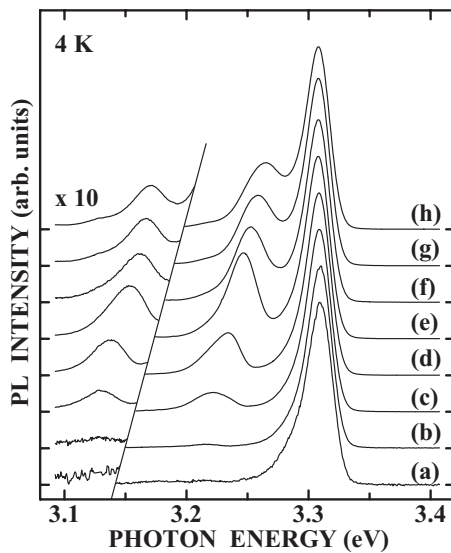


FIG. 3. Photoluminescence spectra at 4 K taken from an $\text{In}_{0.03}\text{Ga}_{0.97}\text{N}$ epitaxial layer under excitation-power densities of (a) 0.0045 , (b) 0.045 , (c) 0.23 , (d) 0.45 , (e) 2.3 , (f) 9.0 , (g) 23 , and (h) 45 W/cm^2 . Each spectrum is normalized at the peak height of the higher-energy component.

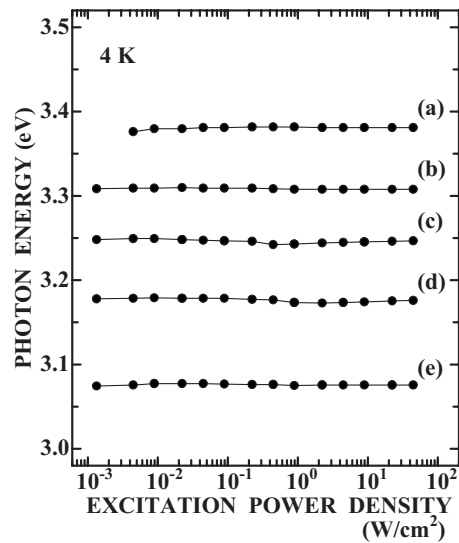


FIG. 4. Photoluminescence-peak photon energy of the higher-energy component at 4 K taken from $\text{In}_x\text{Ga}_{1-x}\text{N}$ epitaxial layers with indium compositions of (a) $x=0.02$, (b) $x=0.03$, (c) $x=0.05$, (d) $x=0.06$, and (e) $x=0.09$ as a function of excitation-power density.

dependent PL-peak photon energy at 4 K of the higher- and the lower-energy components, respectively, for $\text{In}_x\text{Ga}_{1-x}\text{N}$ epitaxial layers with indium compositions of (a) $x=0.02$, (b) $x=0.03$, (c) $x=0.05$, (d) $x=0.06$, and (e) $x=0.09$. The PL-peak position of the higher-energy component for all five samples is almost constant and is independent of the excitation-power density. In contrast, in all five samples, the lower-energy component shifts toward higher energy with increasing excitation-power density. The blueshift is larger for the samples with higher indium compositions.

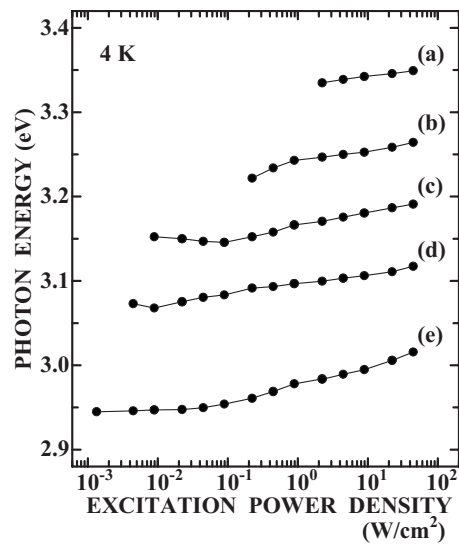


FIG. 5. Photoluminescence-peak photon energy of the lower-energy component at 4 K taken from $\text{In}_x\text{Ga}_{1-x}\text{N}$ epitaxial layers with indium compositions of (a) $x=0.02$, (b) $x=0.03$, (c) $x=0.05$, (d) $x=0.06$, and (e) $x=0.09$ as a function of excitation-power density.

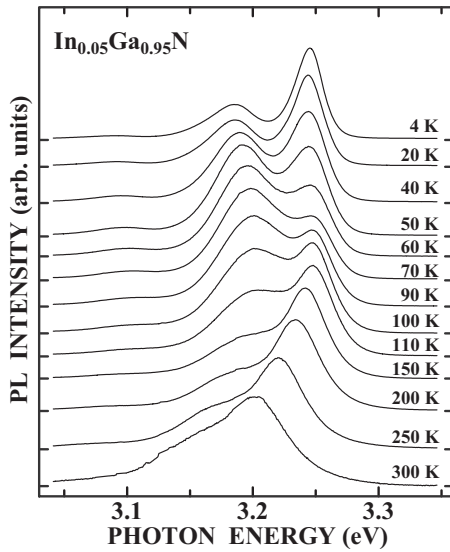


FIG. 6. Temperature dependence of photoluminescence spectra taken from an $\text{In}_{0.05}\text{Ga}_{0.95}\text{N}$ epitaxial layer from 4 to 300 K under an excitation-power density of 45 W/cm^2 . Each spectrum is normalized at the peak height of the higher-energy component.

C. Temperature dependence of PL spectra

Figure 6 shows the temperature dependence of the PL spectra taken from the $\text{In}_{0.05}\text{Ga}_{0.95}\text{N}$ epitaxial layer from 4 to 300 K under an excitation-power density of 45 W/cm^2 . Each PL spectrum is normalized at the peak height of the higher-energy component. With increasing temperature from 4 K to about 70 K, the PL intensity of the lower-energy component relative to that of the higher-energy component increases gradually, and the lower-energy component becomes prominent. With further increase in temperature, it begins to decrease and the PL spectrum at 300 K is dominated again by the higher-energy component. Such temperature dependence indicates that the radiative recombination channels of the two components are not independent of each other and that thermal population of carriers between the two components takes place. We observed a similar temperature dependence of the PL spectra for the four other samples with different indium compositions. Figure 7 shows the temperature-dependent PL intensity ratio of the lower-energy component (I_{LEC}) relative to the higher-energy component (I_{HEC}) for three samples with indium compositions of (a) $x=0.02$, (b) $x=0.05$, and (c) $x=0.09$. The ratio for each sample is normalized at the maximum value. For the sample with the indium composition of $x=0.02$, the ratio increases with increasing temperature and reaches its maximum value at 40 K. Subsequently, the ratio decreases with further increase in temperature. The temperature at which the ratio reaches its maximum becomes higher with increasing indium composition, 75 K for $x=0.05$ and 110 K for $x=0.09$.

D. Near-field PL

The macroscopic PL measurements described above indicate that the band-edge PL from $\text{In}_x\text{Ga}_{1-x}\text{N}$ ternary alloys consists of two intrinsic emission components. In order to

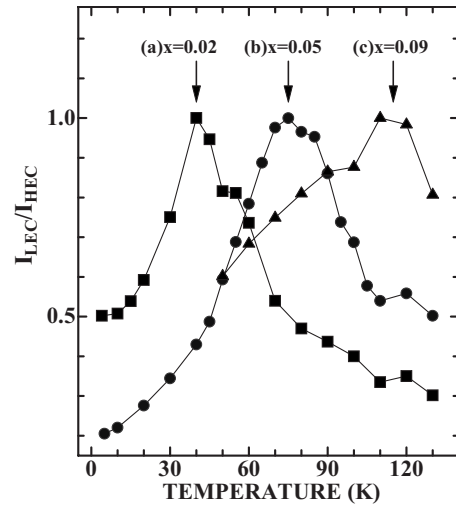


FIG. 7. Temperature-dependent photoluminescence intensity ratio of the lower-energy component relative to the higher-energy component taken from three $\text{In}_x\text{Ga}_{1-x}\text{N}$ epitaxial layers with indium compositions of (a) $x=0.02$, (b) $x=0.05$, and (c) $x=0.09$.

study the spatial distribution of the PL, we performed SNOM-PL measurements. Figure 8 shows near-field PL intensity images at 36 K taken from $\text{In}_x\text{Ga}_{1-x}\text{N}$ epitaxial layers with indium compositions of (a) $x=0.02$, (b) $x=0.03$, (c) $x=0.05$, (d) $x=0.06$, and (e) $x=0.09$ under the illumination and collection hybrid mode using a fiber probe with an aperture diameter of 110 nm. The images were obtained from a $2 \times 2 \mu\text{m}^2$ area with a probing step of 50 nm. The near-field PL intensity increases with increasing indium composition, and the bright regions become larger and an islandlike distribution becomes prominent.

To further clarify the spatial distribution of the two emission components, the near-field PL intensity images monitored at the PL-peak energy of both the higher- and the lower-energy components are shown in Figs. 9(a) and 9(b), respectively, for the sample with an indium composition of $x=0.05$. The images shown in Figs. 9(a) and 9(b) are derived from the image shown in Fig. 8(c). The higher-energy component observed at 3.247 eV corresponds to islandlike regions with diameters of several hundred nanometers. In contrast, the lower-energy component observed at 3.191 eV corresponds to dotlike regions with diameters less than 100 nm, which is limited by the spatial resolution (aperture diameter of 110 nm). In addition, the lower-energy component is observed in the region where the intensity of the higher-energy component is extremely weak, as shown in Figs. 9(a) and 9(b) by the dashed circles. This observation unambiguously indicates a spatial separation between the regions corresponding to the higher- and the lower-energy components. A similar spatial separation was observed for the samples with indium compositions of $x=0.03$, 0.06, and 0.09, although it could not be clearly detected for the sample with an indium composition of $x=0.02$. This is because, for the latter case, the islandlike distribution is less pronounced owing to the small potential fluctuation and small energy separation between the higher- and the lower-energy components.

To gain a more detailed insight into the spatial distribution of both components, we performed a similar SNOM mea-

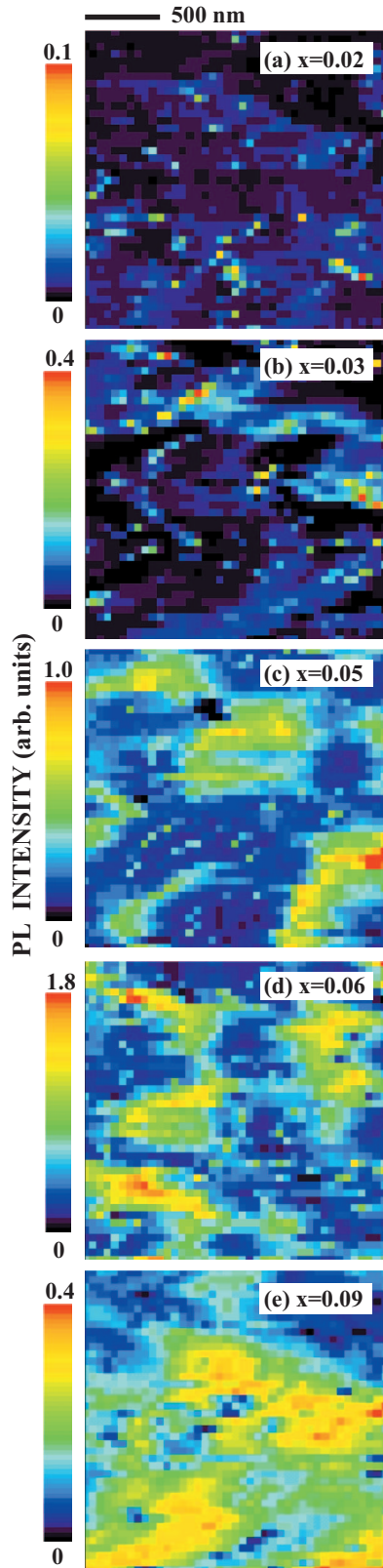


FIG. 8. (Color) Near-field photoluminescence intensity images at 36 K taken from $\text{In}_x\text{Ga}_{1-x}\text{N}$ epitaxial layers with indium compositions of (a) $x=0.02$, (b) $x=0.03$, (c) $x=0.05$, (d) $x=0.06$, and (e) $x=0.09$ under the illumination and collection hybrid mode using a fiber probe with an aperture diameter of 110 nm. Each image is obtained from a $2 \times 2 \mu\text{m}^2$ area with a probing step of 50 nm.

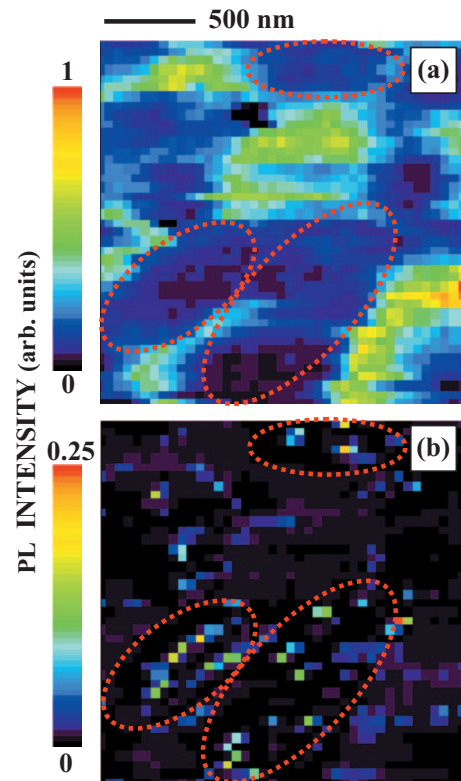


FIG. 9. (Color) Near-field photoluminescence intensity images at 36 K taken from an $\text{In}_{0.05}\text{Ga}_{0.95}\text{N}$ epitaxial layer under the illumination and collection hybrid mode using a fiber probe with an aperture diameter of 110 nm. Images (a) and (b) are obtained by mapping the photoluminescence intensity of the higher- and the lower-energy components, respectively.

surement under higher spatial resolution. Figures 10(a) and 10(b) show the near-field PL intensity images monitored at the PL-peak energy of the higher- and the lower-energy components, respectively, for the sample with an indium composition of $x=0.05$, taken at 25 K using a fiber probe with an aperture diameter of 30 nm. The images were obtained from a $600 \times 600 \text{ nm}^2$ area with a probing step of 15 nm. As seen in Fig. 10(b), the spatial extent of the regions corresponding to the lower-energy component is about 50–80 nm. From Fig. 10(a) it is also seen that the PL intensity of the higher-energy component is weak in the region of not only the bright spots of the lower-energy component themselves (solid circles) but also the areas surrounding these spots (dashed circles).

IV. DISCUSSION

In semiconductor ternary alloys, the energy states of excitons are broadened inhomogeneously by alloy compositional fluctuation. Initially created excitons are therefore localized at the lower-energy states of the inhomogeneously broadened exciton resonance. The first experimental evidence of exciton localization by alloy fluctuation was reported by Lai and Klein for indirect gap $\text{GaAs}_{1-x}\text{P}_x$.²⁴ Subsequently, such localization has been studied for direct-gap II–VI ternary alloys with anion substitution such as $\text{CdS}_{1-x}\text{Se}_x$ (Refs. 25 and 26) and with cation substitution

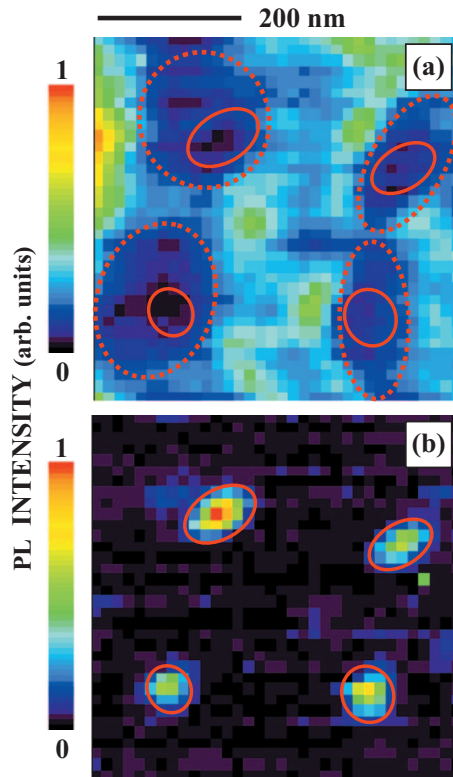


FIG. 10. (Color) Near-field photoluminescence intensity images at 25 K taken from an $\text{In}_{0.05}\text{Ga}_{0.95}\text{N}$ epitaxial layer under the illumination and collection hybrid mode using a fiber probe with an aperture diameter of 30 nm. Images (a) and (b) are obtained by mapping the photoluminescence intensity of the higher- and the lower-energy components, respectively.

such as $\text{Zn}_{1-x}\text{Cd}_x\text{S}$ (Ref. 27) systems. The general picture of exciton motion in semiconductor ternary alloys has well been explained as follows.²⁸ At intraband excitation excitons are created in the high density of states region and have a kinetic energy far exceeding the amplitude of the crystal-potential fluctuation. Such excitons do not see the potential fluctuation and can be regarded as free particles. Therefore, the excitons have a high probability of spatial migration. Energy relaxation through the emission of phonons brings the excitons into the energy region of random potential relief where further energy relaxation and spatial migration are possible only through tunneling into localized states with lower energy. Namely, at kinetic energies comparable with potential fluctuation, the spatial localization of excitons can take place in the wells of the crystal potential. The states of localized and delocalized (free or extended) excitons are separated by some characteristic energy, the so-called mobility edge, which corresponds to the general Mott-Anderson model in disordered systems. When the thermal energy ($k_B T$) becomes comparable to the localization energy of excitons, the population of excitons changes from localized states to delocalized (extended) states, at which point the excitons behave similarly to free excitons in binary materials.

In the case of $\text{In}_x\text{Ga}_{1-x}\text{N}$ ternary alloys, our experimental observations cannot be explained solely by the general model of exciton localization mentioned above. One of the most notable features is the existence of the two intrinsic

emission components, that is, the strong higher-energy and the weak lower-energy components. The two emission components have the following features: first, the lower-energy component has a strong LO-phonon coupling compared to the higher-energy component. This is because the PL intensity of the LO-phonon replica for the lower-energy component is stronger than that for the higher-energy component, though the PL intensity of the lower-energy component itself is weaker than that of the higher-energy component.

Second, the excitation-power-density-dependent PL measurements indicate that the lower-energy component shifts to higher energy with increasing excitation-power density, and the PL intensity of the lower-energy component is saturated at higher excitation-power density. Therefore, it is reasonable to understand that the inhomogeneous broadening is larger and the density of states is lower for the lower-energy component than for the higher-energy component. In addition, the PL intensity of the lower-energy component is extremely weak at lower excitation-power density. This indicates that the effect of nonradiative recombination for the lower-energy component is larger than that for the higher-energy component.

Third, based on the temperature dependence of the PL spectra, it is reasonable to assume that the radiative recombination channels of the two emission components are not independent and that thermal population of carriers occurs between the two components. It is found from the time-resolved PL measurements that, just after excitation, an energy transfer from the higher-energy to the lower-energy component takes place within several tens of picoseconds.¹⁷ It is also found from the PLE measurement that the carriers responsible for the two emission components are relaxed from the same excited state.¹⁸ These experimental observations are consistent with the above-mentioned assignment based on the temperature-dependent PL measurements. Cho *et al.*²⁹ reported that the temperature dependence of PL spectra for InGaN/GaN QWs exhibited an abnormal peak shift with a S-shaped character, as if the PL spectrum was a single emission band. However, on the basis of the experimental results mentioned above, such behavior does not originate from the abnormal temperature dependence but is instead due to the existence of the two intrinsic emission components. Furthermore, the temperature-dependent OA results indicate that the Stokes shift of both components is independent of temperature above 100 K and is almost constant up to RT.¹⁹ This suggests the strong localization of excitons, even at RT.

Fourthly, the SNOM-PL measurements yield the important result that there is a spatial separation between the higher- and the lower-energy components. In particular, the PL intensity of the higher-energy component is weak not only at the bright spots corresponding to the lower-energy component but also in surrounding areas. In the SNOM-PL measurements under the illumination and collection hybrid mode, when the microscopic area of local potential minima is measured, most of the photogenerated carriers remain under the probing aperture. In this case, the detected PL intensity is strong. In contrast, when the microscopic area of local potential maxima is measured, most of the photogenerated carriers immediately relax to local potential minima, that is,

outside of the probing aperture, and the detected PL intensity is weak. Therefore, we consider that regions corresponding to the lower-energy component, with dimensions of 50–80 nm, are surrounded by local potential maxima as shown in Fig. 10(a) by the dashed circles. This implies that a potential barrier exists between regions corresponding to the higher- and the lower-energy components. Such a potential barrier is related to the thermal population of carriers between the two emission components, as observed in the temperature-dependent PL spectra shown in Fig. 6. Then, the height of the potential barrier seems to become higher with increasing indium composition because the temperature at which the PL intensity ratio ($I_{\text{LEC}}/I_{\text{HEC}}$) reaches its maximum becomes higher, as shown in Fig. 7.

On the basis of these findings, it is interesting to consider the possible origin of the higher-energy component. It is reasonable to understand that excitons in $\text{In}_x\text{Ga}_{1-x}\text{N}$ ternary alloys are subject to localization due to alloy disorder, which results in the inhomogeneous broadening of the exciton density of states. However, it should be noted again that the radiative recombination process for the band-edge PL from $\text{In}_x\text{Ga}_{1-x}\text{N}$ ternary alloys cannot be explained solely by this simple model, as evidenced by the temperature-independent Stokes shift.¹⁹ If exciton localization originates from inhomogeneous broadening due to compositional fluctuation, the Stokes shift should gradually decrease with increasing temperature because of the thermal population of excitons from localized to extended states. However, it is found that the Stokes shift observed above 100 K is almost constant up to RT and increases with indium composition from 19 meV for the sample with $x=0.02$ to 34 meV for the sample with $x=0.09$. This indicates that there is another mechanism of exciton localization in addition to inhomogeneous broadening. One probable mechanism involves strong hole localization.^{30,31} Using empirical pseudopotential calculations, Bellaiche *et al.* reported that alloying of GaN with indium-induced localization in the hole wave function, resonating within the valence band. They pointed out that the hole localization occurred even with a perfectly homogeneous indium distribution, and that such an unusual effect could explain the exciton localization simultaneously.³⁰ Therefore, it is possible that exciton localization due to alloy disorder is effectively enhanced by the strong hole localization in $\text{In}_x\text{Ga}_{1-x}\text{N}$ ternary alloys. Such an enhancement results in the strong exciton localization evidenced by the temperature-independent Stokes shift.

Next, we consider the origin of the lower-energy component. There have been several reports concerning the relation between dislocations and compositional inhomogeneity. Sato *et al.*³² studied the compositional inhomogeneity of InGaN layers by means of CL and energy-dispersive x-ray spectroscopy and reported that dislocations played a key role in producing compositional inhomogeneity in InGaN layers. Duxbury *et al.*³³ directly measured phase segregation in InGaN quantum wells by means of spatially resolved energy-dispersive x-ray analysis in a dedicated scanning transmission electron microscope and reported that indium fluctuations became increasingly pronounced in the vicinity of dislocations. Chen *et al.*³⁴ observed spontaneous formation of nanometer-size compositional fluctuations on InGaN sur-

faces by means of scanning tunneling microscopy. In the present context, we consider that increased indium incorporation around threading dislocations, that is, the formation of local indium-rich regions with diameters of 50–80 nm results in the creation of deeply localized states for excitons, and that these states are responsible for the lower-energy component. Namely, the lower-energy component originates from deep exciton localization at the regions of increased indium incorporation around threading dislocations. This assignment is supported by the fact that the density of dotlike regions corresponding to the lower-energy component is estimated to be $2.0 \times 10^8 \text{ cm}^{-2}$, which is in good agreement with the density of growth pits ($1.7 \times 10^8 \text{ cm}^{-2}$) as well as the density of threading dislocations ($1.5 \times 10^8 \text{ cm}^{-2}$). The assignment is consistent with the fact that the lower-energy component has a strong LO-phonon coupling compared to the higher-energy component, as shown in Fig. 2 because the exciton LO-phonon coupling is enhanced by exciton localization.³⁵ It is also consistent with the fact that the density of states for the lower-energy component is thought to be lower than that for the higher-energy component, and that the effect of the non-radiative recombination process for the lower-energy component is thought to be larger than that for the higher-energy component.

Furthermore, there have been several SNOM studies on the formation of local potential barriers around defects in $\text{In}_x\text{Ga}_{1-x}\text{N}$ ternary-alloy systems.^{14,16} In particular, Hangleiter *et al.*³⁶ reported the formation mechanism of local potential barriers in $\text{In}_x\text{Ga}_{1-x}\text{N}/\text{GaN}$ QWs. They explained that hexagonal V-shaped pits decorating the threading dislocations exhibited sidewall quantum wells with reduced thickness and higher band gap thus leading to a potential barrier around every defect. In the case of our $\text{In}_x\text{Ga}_{1-x}\text{N}$ thick layers (90 nm), however, a different mechanism is needed to explain the formation of local potential barriers. The mechanism is not clear at the present stage. One probable mechanism involves strain due to lattice distortion caused by the formation of local indium-rich regions. It is possible that such strain results in the formation of the potential barrier which surrounds the regions corresponding to the lower-energy component, that is, the local indium-rich regions.

V. CONCLUSIONS

We have studied the characteristics of band-edge PL from Ga-rich $\text{In}_x\text{Ga}_{1-x}\text{N}$ ternary-alloy epitaxial layers using SNOM in addition to conventional macroscopic PL spectroscopy. The band-edge PL from the ternary alloys consisted of two intrinsic emission components. The spatial separation between the two components was clearly indicated by SNOM-PL measurements. Regions corresponding to the higher-energy component had an islandlike distribution with diameters of several hundred nanometers whereas regions corresponding to the lower-energy component were dotlike with diameters of 50–80 nm. The lower-energy component originated from deep exciton localization at the regions of increased indium incorporation around threading dislocations. Therefore, the spatially separated two emission components resulted from different indium incorporation close to and far from threading dislocations. In addition, the regions

corresponding to the lower-energy component were surrounded by local potential maxima, which acted as a potential barrier for carriers between the higher- and the lower-energy components.

ACKNOWLEDGMENTS

One of the authors (Y.Y.) would like to thank Yoichi Kawakami of Kyoto University for valuable discussions. The

authors would also like to thank Narihito Okada of Yamaguchi University for AFM measurements, and Chiharu Sasaki, Hiroki Ishibashi, and Masaki Iwata for their help. This work was partly supported by a Grant-in-Aid for Scientific Research on Priority Areas No. 19032007 and No. 21016005 and the Knowledge Cluster Initiative from the Ministry of Education, Culture, Sports, Science and Technology of Japan.

*Corresponding author; yamada@yamaguchi-u.ac.jp

- ¹S. D. Lester, F. A. Ponce, M. G. Craford, and D. A. Steigerwald, *Appl. Phys. Lett.* **66**, 1249 (1995).
- ²S. Chichibu, T. Azuhata, T. Sota, and S. Nakamura, *Appl. Phys. Lett.* **69**, 4188 (1996).
- ³Y. Narukawa, Y. Kawakami, Sz. Fujita, Sg. Fujita, and S. Nakamura, *Phys. Rev. B* **55**, R1938 (1997).
- ⁴P. A. Crowell, D. K. Young, S. Keller, E. L. Hu, and D. D. Awschalom, *Appl. Phys. Lett.* **72**, 927 (1998).
- ⁵D. K. Young, M. P. Mack, A. C. Abare, M. Hansen, L. A. Coldren, S. P. Denbaas, E. L. Hu, and D. D. Awschalom, *Appl. Phys. Lett.* **74**, 2349 (1999).
- ⁶A. Vertikov, M. Kuball, A. V. Nurmikko, Y. Chen, and S.-Y. Wang, *Appl. Phys. Lett.* **72**, 2645 (1998).
- ⁷A. Vertikov, A. V. Nurmikko, K. Doverspike, G. Bulman, and J. Edmond, *Appl. Phys. Lett.* **73**, 493 (1998).
- ⁸A. Vertikov, I. Ozden, and A. V. Nurmikko, *Appl. Phys. Lett.* **74**, 850 (1999).
- ⁹M. S. Jeong, J. Y. Kim, Y.-W. Kim, J. O. White, E.-K. Suh, C.-H. Hong, and H. J. Lee, *Appl. Phys. Lett.* **79**, 976 (2001).
- ¹⁰M. S. Jeong, Y.-W. Kim, J. O. White, E.-K. Suh, M. G. Cheong, C. S. Kim, C.-H. Hong, and H. J. Lee, *Appl. Phys. Lett.* **79**, 3440 (2001).
- ¹¹J. Kim, K. Samiee, J. O. White, J.-M. Myoung, and K. Kim, *Appl. Phys. Lett.* **80**, 989 (2002).
- ¹²A. Kaneta, K. Okamoto, Y. Kawakami, S. Fujita, G. Marutsuki, Y. Narukawa, and T. Mukai, *Appl. Phys. Lett.* **81**, 4353 (2002).
- ¹³A. Kaneta, T. Mutoh, Y. Kawakami, Sg. Fujita, G. Marutsuki, Y. Narukawa, and T. Mukai, *Appl. Phys. Lett.* **83**, 3462 (2003).
- ¹⁴F. Hitzel, G. Klewer, S. Lahmann, U. Rossow, and A. Hangleiter, *Phys. Rev. B* **72**, 081309 (2005).
- ¹⁵Y. Kawakami, K. Nishizuka, D. Yamada, A. Kaneta, M. Funato, Y. Narukawa, and T. Mukai, *Appl. Phys. Lett.* **90**, 261912 (2007).
- ¹⁶A. Kaneta, M. Funato, and Y. Kawakami, *Phys. Rev. B* **78**, 125317 (2008).
- ¹⁷H. Kudo, H. Ishibashi, R. Zheng, Y. Yamada, and T. Taguchi, *Phys. Status Solidi B* **216**, 163 (1999).
- ¹⁸H. Kudo, K. Murakami, H. Ishibashi, R. Zheng, Y. Yamada, and T. Taguchi, *Phys. Status Solidi B* **228**, 55 (2001).
- ¹⁹C. Sasaki, H. Naito, M. Iwata, H. Kudo, Y. Yamada, T. Taguchi, T. Jyouichi, H. Okagawa, K. Tadatomo, and H. Tanaka, *J. Appl. Phys.* **93**, 1642 (2003).
- ²⁰T. Takeuchi, H. Takeuchi, S. Sota, H. Sakai, H. Amano, and I. Akasaki, *Jpn. J. Appl. Phys., Part 2* **36**, L177 (1997).
- ²¹K. Hiramatsu, Y. Kawaguchi, M. Shimizu, N. Sawaki, T. Zhel'eva, R. F. Davis, H. Tsuda, W. Taki, N. Kuwano, and K. Oki, *MRS Internet J. Nitride Semicond. Res.* **2**, 6 (1997).
- ²²K. Tadatomo, H. Okagawa, Y. Ohuchi, T. Tsunekawa, Y. Imada, M. Kato, and T. Taguchi, *Jpn. J. Appl. Phys., Part 2* **40**, L583 (2001).
- ²³T. Saiki and K. Matsuda, *Appl. Phys. Lett.* **74**, 2773 (1999).
- ²⁴S. Lai and M. V. Klein, *Phys. Rev. Lett.* **44**, 1087 (1980).
- ²⁵S. Permogorov, A. Reznitskii, S. Verbin, G. O. Müller, P. Flögel, and M. Nikiforova, *Phys. Status Solidi B* **113**, 589 (1982).
- ²⁶E. Cohen and M. D. Sturge, *Phys. Rev. B* **25**, 3828 (1982).
- ²⁷Y. Kawakami, M. Funato, Sz. Fujita, Sg. Fujita, Y. Yamada, and Y. Masumoto, *Phys. Rev. B* **50**, 14655 (1994).
- ²⁸S. Permogorov and A. Reznitsky, *J. Lumin.* **52**, 201 (1992).
- ²⁹Y.-H. Cho, G. H. Gainer, A. J. Fischer, J. J. Song, S. Keller, U. K. Mishra, and S. P. DenBaars, *Appl. Phys. Lett.* **73**, 1370 (1998).
- ³⁰L. Bellaiche, T. Mattila, L.-W. Wang, S.-H. Wei, and A. Zunger, *Appl. Phys. Lett.* **74**, 1842 (1999).
- ³¹P. R. C. Kent and A. Zunger, *Appl. Phys. Lett.* **79**, 1977 (2001).
- ³²H. Sato, T. Sugahara, Y. Naoi, and S. Sakai, *Jpn. J. Appl. Phys., Part 1* **37**, 2013 (1998).
- ³³N. Duxbury, U. Bangert, P. Dawson, E. J. Thrush, W. Van der Stricht, K. Jacobs, and I. Moerman, *Appl. Phys. Lett.* **76**, 1600 (2000).
- ³⁴H. Chen, R. M. Feenstra, J. E. Northrup, T. Zywietz, and J. Neugebauer, *Phys. Rev. Lett.* **85**, 1902 (2000).
- ³⁵M. S. Skolnick, K. J. Nash, P. R. Tapster, D. J. Mowbray, S. J. Bass, and A. D. Pitt, *Phys. Rev. B* **35**, 5925 (1987).
- ³⁶A. Hangleiter, F. Hitzel, C. Netzelt, D. Fuhrmann, U. Rossow, G. Ade, and P. Hinze, *Phys. Rev. Lett.* **95**, 127402 (2005).